## ABSTRACT

RIVERS, NATHANIEL ALBERT. Progress Towards Synthesis and Characterization of Vinyl- and Ethynyl-Bridged Donor-Acceptor Biradical Complexes. (Under the direction of Dr. David A. Shultz).

Realization of single-molecule devices requires understanding of specific electronic structures and their relationships with device function. Many simple chemical functional groups can act as components of such devices, but studies that definitively measure certain functional group's capacity to transmit electronic information remain scarce. Surprisingly, it is unknown precisely the relative magnitudes of electronic- or magnetic coupling provided by simple vinyl and ethynyl groups. Double bonds and triple bonds are heavily utilized in the fields of photonics and molecular electronics as bridging units that facilitate electron- or exciton transfer generally between two specific locations in a molecule. Herein, we seek to understand the electronic coupling of these two functional groups which lay the foundation for their utility in single-molecule devices. Specifically, the synthesis and characterization of semiquinone (SQ) radicals containing vinyl and ethynyl moieties is discussed. These molecules along with semiquinone - nitronyl nitroxide (NN) biradicals will provide a deeper understanding of electronic coupling provided by these simple, but important functional groups.

# Progress Towards Synthesis and Characterization of Vinyl- and Ethynyl-Bridged Donor-Acceptor Biradical Complexes

by
Nathaniel Albert Rivers

A thesis submitted to the Graduate Faculty of
North Carolina State University
in partial fulfillment of the
requirements for the degree of
Master of Science

Chemistry

Raleigh, North Carolina
2019

APPROVED BY:

| | |
|---|---|
| _____ | _____ |
| David A. Shultz | Felix Castellano |
| Chair of Advisory Committee | |
| _____ | |
| Christopher Gorman | |

## DEDICATION

To my loving wife.

## BIOGRAPHY

Nathaniel Albert Rivers was born in 1993 to his parents, Dave Rivers and Karen Abrams in Raleigh, North Carolina. Nathan was raised in Raleigh and graduated from Sanderson High School in 2012. He attended Furman University for undergraduate studies and completed his B.S. in Chemistry in 2016. He began graduate school in 2017 at North Carolina State University, studying under Dr. David A. Shultz. He married Alexandra Scott in September of 2018. In May of 2019, Nathan will earn his M.S. from North Carolina State University.

# TABLE OF CONTENTS

# LIST OF TABLES

## LIST OF FIGURES

# CHAPTER 1

## Introduction

**Introduction to Electron Coupling**

Electron transfer and exchange coupling are interrelated and crucial to the design of new magnetic, molecular electronic/spintronic, single molecule, and photovoltaic devices. Generally, electron transfer incorporates oxidation-reduction processes between an electron rich donor and electron poor receptor. The exact nature of factors that govern electron transfer has been a field of intense study for over six decades. The "magnetic" interaction between a paramagnetic ($S \geq 1/2$) electron donor and a paramagnetic acceptor, called magnetic exchange coupling, can be understood as the interaction between magnetic moments of unpaired electrons and an expanded definition will be provided Section II.3. Reports of the relationship between magnetic exchange coupling and electron transfer processes are few and far between due to the difficulty in directly measuring exchange coupling (particularly in excited states) and often only measured for inorganic systems comprised of transition metal ions such as Fe, Ni, or Co in various oxidation states.[13] For some time, organics have been touted as useful materials for nanoelectronics due to their synthetic flexibility and attractive physical properties as well as for the belief that silicon-based microelectronics will reach a limit of miniaturization.[1] In order to design organic molecules for these applications, fundamental molecular structure-property relationships must be elucidated.

In 1956, Marcus correlated the kinetics of electron transfer to the thermodynamics of the process in his namesake equation in which the rate constant *k* of an electron transfer reaction between a donor D and acceptor A is given by Equation I.1 where $H_{DA}$ is the electronic coupling matrix element between donor and acceptor.[2]

$$K_{D\to A} = \frac{|H_{DA}|^2}{\hbar\pi^2\sqrt{\lambda k_B T}} \exp\left(\frac{-\lambda + \Delta_r G^0}{4k_B T}\right)^2 \qquad (I.1)$$

Marcus defined $H_{DA}$ as a measure that quantified the amount of exchange between donor and acceptor, or more precisely, the $H_{DA}$ is the electronic matrix element describing the electronic coupling of the reactants' electronic state with that of the product.[3-5] McConnell's definition of $H_{DA}$ is ubiquitous in the literature and expresses $H_{DA}$ as a product of resonance integrals modulated by the energy gap between donor and bridge orbitals.[6] His expression of $H_{DA}$ for a multibridge system is given in Equation I.2 where $H_{BB}$ is the bridge-bridge coupling element and *N* is number of bridging units. $H_{DA}$ is modulated by the energy gap between interacting fragments and is a parameter of delocalization between donor and acceptor that is affected by a bridging unit. If there is no bridge between donor and acceptor, N = 0, then there is no bridging function in the equation. $H_{DA}$ is therefore a link between electron transfer rate, molecular structure, and since the resonance integral is often conformation-dependent, molecular conformation. As such, understanding molecular structure-property relationships of $H_{DA}$ is the guiding principle for rational design of electron transfer architectures and is key in developing nanoelectronics, photonics and molecule-based magnetic materials.[15] This section will focus on evaluation of H and use it to determine electronic structure-property relationships.

$$H_{DA} = \frac{H_{DB}H_{BA}}{\Delta E_{DB}}\left(\frac{H_{BB}}{H_{DA}}\right)^{N-1} \qquad \text{(I. 2)}$$

Currently, H cannot be measured directly. However, there are several techniques which can probe it indirectly. Using magnetic field dependent electron transfer (ET) kinetics to probe photoactive donor-bridge-acceptor (D-B-A) molecules that undergo a photoinduced electron transfer event (PET) is a well-documented method of determining H.[2,16] Upon photoexcitation, a D-B-A system will generate a $D^*$-B-A excited state which then undergoes intramolecular ET to yield the zwitterionic $D^+$-B-$A^-$ charge-separated state (which is also a biradical). This charge-separated state can energetically decay back to the ground D-B-A state and using ultrafast

transient absorption spectroscopy, the rates of charge separation and recombination can be determined. By comparing the photoinduced electron transfer rates in different magnetic fields, the excited singlet-triplet gap can be determined, and H can be estimated through Equation I.3.

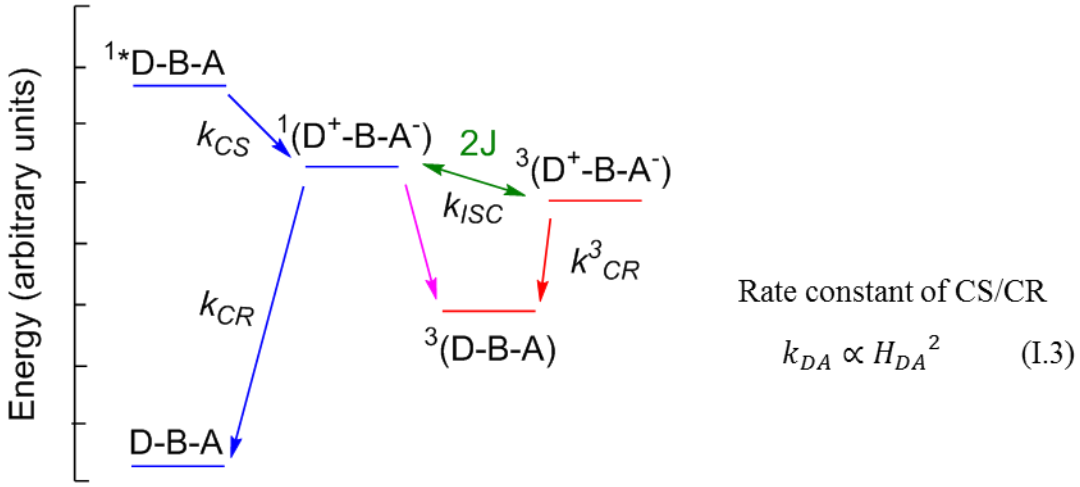


**Figure I.1.** Jablonski diagram of generic DBA moiety that undergoes a photoinduced electron transfer event. $K_{CS}$ is the charge separation rate constant, $k_{ISC}$ is the intersystem crossing rate constant between singlet and triplet states, and $k_{CR}$ is the charge recombination rate constant.

However, this technique requires very weak coupling in short-lived excited states which cannot be structurally characterized. This leaves the correlation between structure and coupling somewhat ambiguous.

Another experiment that allows indirect determination of H is performing metal-molecule-metal break-junction conductance experiments. Landauer correlated conductance ($g$) with H as shown in Equation I.4 which also shows that electron transmission is controlled by electronic coupling with the donor and acceptor electrodes ($\Gamma_D$ and $\Gamma_A$).[7-9]

$$g = \frac{e^2}{\pi\hbar}|H_{DA}|^2\Gamma_D\Gamma_A \qquad \text{(I. 4)}$$

Break-junction conductance experiments involve placing a molecule of interest between two nanoelectrodes, often gold or platinum, and then repeatedly moving the electrodes closer together and farther apart using a piezoelectric motor or an STM probe tip.[10,14] At certain

distances, molecules are trapped between the electrodes and their I-V characteristics can be measured. The molecule of interest is usually covalently bonded to metal surface anchoring functional groups, such as thiols for gold electrodes. This system can determine the average conductance of one analyte rather reliably through multiple measurements. Naturally as samples are small and uncontrollable, this method requires multiple data sets, on the order of thousands as a minimum. Today's instruments can perform these measurements in a matter of minutes, however, this still creates uncertainty of the actual analyte orientation and can only provide an averaged value of conductance. Moreover, the structural details of molecular conformation and how the surface attachment groups are bound to the metal surface are unknown.

Nitzan and Ratner correlated electron transfer and conductance by showing that both were proportional to $H^2$. Thus, providing Equation I.5.[10-11]

$$g \sim k_{D\rightarrow A} \sim {H_{DA}}^2 \qquad (\mathrm{I}.5)$$

Donor-Acceptor molecules whose ground states have two unpaired electrons (biradicals) have been proven useful for evaluating H. Anderson demonstrated in Equation I.6 that the magnetic exchange parameter, *J*, which measures the magnetic coupling between unpaired electrons H and can be directly measured by EPR Spectroscopy, variable-temperature magnetic susceptibility, and electronic absorption spectroscopy.[12-13] The Shultz group has correlated *J* in ground-state biradicals with $H_{DA}$ through a wide array of organic bridges. The variety of molecular structure-property relationships demonstrated will be discussed in Chapter 3.

$$2J = \frac{{H_{DA}}^2}{\Delta\varepsilon} \qquad (\mathrm{I}.6)$$

## REFERENCES


(1) Ventra, M. Di; Pantelides, S. T.; Lang, N. D.; *Phys. Rev. Lett.* **2000**, 84, 979

(2) Marcus *J. Chem. Phys.* **1956**, 24, 966;

(3) Marcus, R. A.; Sutin, Norman. *Biochimica et Biophysica Acta,* **1985**, 811, 265-322

(4) Closs, Miller. *J. Am. Chem.* Soc. **1984**, 106, 3049;

(5) McClosky, Winkler, Gray. *J. Am. Chem. Soc.* **1992**, *111*, 6935.

(6) McConnell. Harden M. *J. Chem. Phys.* **1961**, *35*, 508.

(7) Nitzan, A. *J. Phys. Chem. A.* **2001**, 105, 2677-2679;

(8) Landauer, R. *IBM J. Res. DeV.* **1957**, 1, 223

(9) Landauer, R. Philosophical Magazine. **1970**, 21:172, 863-867

(10) Nitzan *J. Phys. Chem. A.* **2001,** *105*, 2677;

(11) Ratner. *Nature Nanotechnology* **2013**, *8*, 378-381.

(12) Anderson. *Phys. Rev.* **1959**, *115*, 2;

(13) Wasielewski, *et al. J. Am. Chem. Soc.* **2003**, *125*, 3921.

(14) Reed, M., *Adv. Mater.* Vol. 23, 14, **2011,** 1583–1608

(15) Kirk, M. L.; Shultz, *et al*. L. *J. Am. Chem. Soc.* **2007**, *129*, 1937.

(16) Wasielewski, M. R. *et al. J. Phys. Chem. B* **2006**, *110*, 25163

# Chapter 2

## Valence Bond Configuration Interaction Model for Magnetic- and Electronic Coupling in a Two-spin System

**II.1 Donor-Bridge-Acceptor System**

The Shultz group ground-state biradical system, described in further detail in Section II.2, differs significantly from other methods used to determine $H_{DA}$ such as magnetic-field dependent photoinduced electron transfer (PET) studies or break-junction conductance and provides a number of advantages as a platform for evaluating electronic structure contributions to $H_{DA}$. The biradical model can directly measure *J* in the ground state while not relying on undefined electronic structures of excited states.[1] The biradicals used are able to be crystallized and therefore allow precise structure and conformation determination by X-ray crystallography. The sign of the exchange parameter, *J* is also measured, and is useful in determining superexchange pathways.[1] The ability to measure the sign and magnitude of *J* for any synthetically-viable structure is particularly useful for understanding single-molecule current rectification, since our biradical molecules can be considered analogs of single molecule electronic devices (*vide infra*).[2]

Donor-Bridge-Acceptor (D-B-A) systems are molecular 'diodes' comprised of an electron rich donor, a molecular bridge fragment, and an electron-poor acceptor.[2] This connectivity pattern creates a preferred direction for electron flow in charge transfer (CT) steps yet the Shultz system does not utilize CT events to evaluate H, although intra-ligand D→A charge transfer (ILCT) does play a role in superexchange-mediated magnetic exchange.[3] The superexchange effect is further expanded upon in Section II.3. The bridging unit covalently attached to both donor and acceptor units, mediates coupling between the donor and acceptor and controls electron transfer, transport, or when the donor and acceptor are paramagnetic, the magnetic exchange coupling. Synthetic variation of the bridge has been the focus of much work up to this point and requires understanding of $H_{DA}$ and how various bridges affect it.

## II.1 Shultz D-B-A Architecture

The Shultz group biradical D-B-A system, Figure II.1, makes use of a zinc (II) tris-pyrazolylborate (Tp) metal center/ancillary ligand combination.[4-6] The encapsulating ancillary ligand is cage-like and serves as steric protection from intermolecular interactions in the solid state. In fact, it magnetically insulates the biradical molecules from its neighbors, it is spectroscopically silent in the visible region of the electromagnetic spectrum of interest, it balances charge, and its complexes readily crystallize. The $d^{10}$ $Zn^{II}$ metal center is also diamagnetic so it does not alter the magnetic properties. A coordinated mono-protonated catecholate is oxidized to a semiquinone (SQ) by aerial oxidation after complexation with the zinc ion. Since the SQ is electron rich compared to the nitronyl nitroxide (NN) radical it is coupled to, the SQ is the donor radical of the system, while the NN is the acceptor. The SQ is also a resonance donor, while the NN is a resonance acceptor. The SQ is somewhat air stable

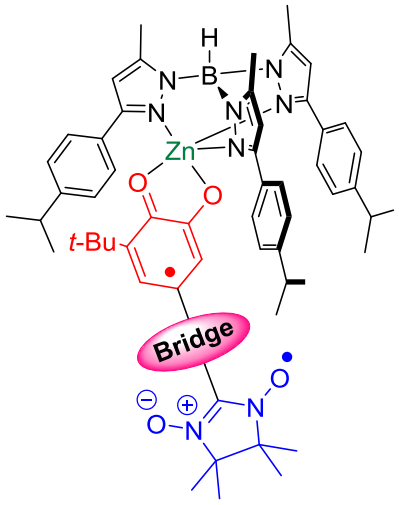


**Figure II.1.** Line bond drawing of Shultz Biradical architecture. (Black) Tris- pyrazolylborate ancillary ligand, (Green) Zn (II) metal center, (Red) Semiquinone, (Pink) any covalently bonded bridge, and (Blue) nitronyl nitroxide.

and has positive spin density at the connection point to the bridge unit. The SQ radical is covalently bonded to a bridging unit which in turn is covalently bonded to the NN radical. What is key, is that the bridging unit can be any synthetically accessible bridge which, at parity of SQ

and NN, allows for direct comparison amongst all bridge units. These molecules can be crystalized and magnetic measurements performed on crystalline samples of known precise geometry and conformation.

### II.3 Superexchange in SQ-Bridge-NN Biradicals

In our biradical system, the interaction between the SQ and NN radicals is governed by superexchange. The two unpaired electrons of the SQ and NN are analogous to a charge separated excited state and are coupled through the bridge.[3] The ground state singlet-triplet gap in our biradicals is derived using a Valence Bond Interaction (VBCI) model in Figure II.2.[8] The lack of orbital overlap between the NN SOMO and SQ SOMO initially suggests degenerate singlet and triplet states ($^1$GC and $^3$GC, respectively) for the ground configuration. This would be true if it were not for excited configurations mixing, via superexchange, with ground configurations. In fact, in excited configurations ($^1$EC and $^3$EC, resulting from SQ SOMO to NN LUMO electronic excitation), mix with $^1$GC and $^3$GC to form the gap defined as 2*J*. For $^1$EC and

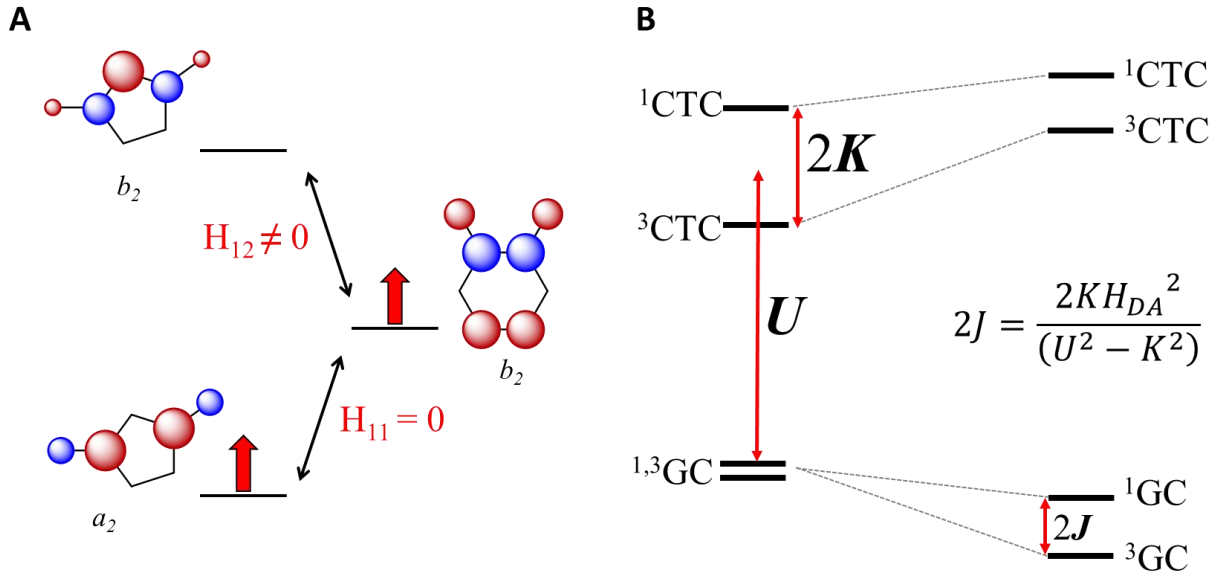


**Figure II.2.** A) Simple Molecular orbital model of SQ and NN HOMO/LUMO interaction. B) State energy diagram with no excited configurations mixing on the left and mixing on right. K is the exchange integral and U is the mean charge transfer energy.

$^3$EC, Hund's Rule dictates that the $^3$EC is lower in energy than the $^1$EC. The smaller energy gap between $^3$EC and $^3$GC compared to $^1$EC and $^1$GC results in $^3$GC lying lower in energy than $^1$CG. As noted above, the gap between $^{1,3}$GC is given as 2*J* and if small compared to $k_BT$, $^1$GC can be thermally populated. Of note, is that the triplet state has a magnetic moment with S = 1 while the

singlet state has S = 0. This is key in measuring *J* from experimental variable-temperature magnetic susceptibility data.

## II.4 Derivation of Spectroscopic Variables

The relationship between *J* and $H_{DA}$ can be understood by first defining that 2*J*, is equal to the energy of the singlet state minus the triplet state (Equation II.1). Perturbation theory, using exchange integral, K, and the mean charge transfer energy (U) between states provides us with Equation II.2.[7]

$$2J = E_s - E_T \tag{II. 1}$$

$$2J = \frac{2K{H_{DA}}^2}{(U^2 - K^2)} \tag{II. 2}$$

Here, K is one-half of the energy difference between the excited $^1$EC and $^3$EC SQ → NN charge-transfer (CT) states and U is the mean CT energy. U and K are spectroscopically available constants which can be determined through estimation using variable-temperature absorption spectroscopy studies.

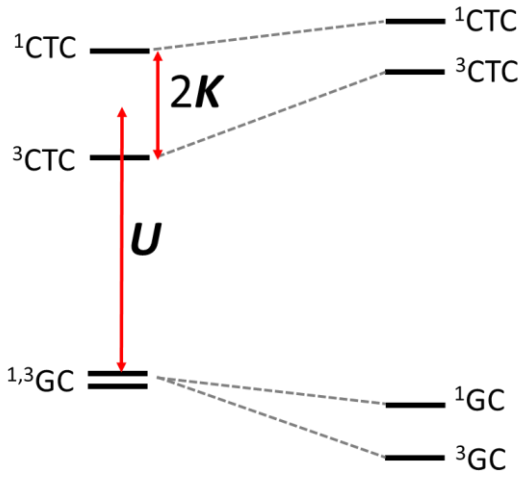


**Figure II.3.** VBCI model of SQ-B-NN biradical interaction.

Variable-temperature magnetic susceptibility data can be used to obtain *J*-values as fit parameters for the biradical system. Most of the SQ-B-NN biradicals reported to date have ground states and their singlet states can be thermally populated. At low temperatures, ~2 K, only the $^3$GC is populated. Using a superconducting quantum interference device (SQUID), a

sample can be slowly warmed and the paramagnetic susceptibility (as the temperature product, $\chi_{para}$•T) will change. Plotting $\chi_{para}$•T vs T allows for determination of 2*J*. Simply substituting directly measured values of 2*J* and spectroscopically available values of U and K into Equation II.2, provides the Shultz group with $H_{DA}$ determined using all experimentally-determined variables.

## REFERENCES

(1) Kirk, M. L.; Shultz, *et al*. *J. Am. Chem. Soc.* **2007**, *129*, 1937.

(2) Kirk, M. L.; Shultz, D. A.; Stasiw, D. E.; Habel-Rodriguez, D.; Stein, B.; Boyle, P. D. *J. Am. Chem. Soc.* **2013**, 135, 14713.

(3) Kirk, M. L.; Shultz, D. A.; Stasiw, D. E.; Lewis, G. F.; Wang, G.; Brannen, C. L.; Sommer, R. D.; Boyle, P. D. *J. Am. Chem. Soc.*, **2013**, 135, 17144.

(4) Shultz, D. A., Bodnar, S. H. *Inorg. Chem.* **1999**, 38, 591-594.

(5) Ruf, M.; Vahrenkamp, H. *Inorg. Chem.* **1996**, 35, 6571.

(6) Ruf, M., et al. *Inorg. Chem.* **1997**, 36, 4860.

(7) Kirk, M. L.; Shultz, D. A.; Depperman, E. C.; Habel-Rodriguez, D.; Schmidt, R. D. *J. Am. Chem. Soc.* **2012**, 134, 7812.

(8) Tuczek, F.; Solomon, E. *I. Coord. Chem. Rev.* **2001**, 219, 1075.

# Chapter III

## Previous Shultz Group Work Related to Structure-Property Relationships of SQ-Bridge-NN Biradical Complexes

**III.1 Distance Dependence Studies.**

An area of recent work reported by the Shultz group focuses on evaluating exchange and electronic coupling as a function of bridge length in D-B-A biradicals.[1] In what was the first direct comparison of $J$ and $H_{DA}$ at parity of donor and acceptor in regard to their distance dependence of various bridging units, the Shultz group found the distance decay constant, $\beta$, for two sets of bridges and that the decay was exponential. This helps to corroborate the SQ → NN superexchange as the dominant pathway for $H_{DA}$ and validates the use of superexchange-mediated VBCI model. A series of $Tp^{Cum,Me}Zn$(SQ-B-NN) with oligo(para-phenylene) and oligo(2,5-thiophene) as bridges, shown in Figure III.1, were synthesized and studied. The $\beta$-values determined compared favorably with those determined for systems with orders of magnitude weaker coupling. In addition, this work also allows measurements to be "corrected" for distance effects in future experiments.

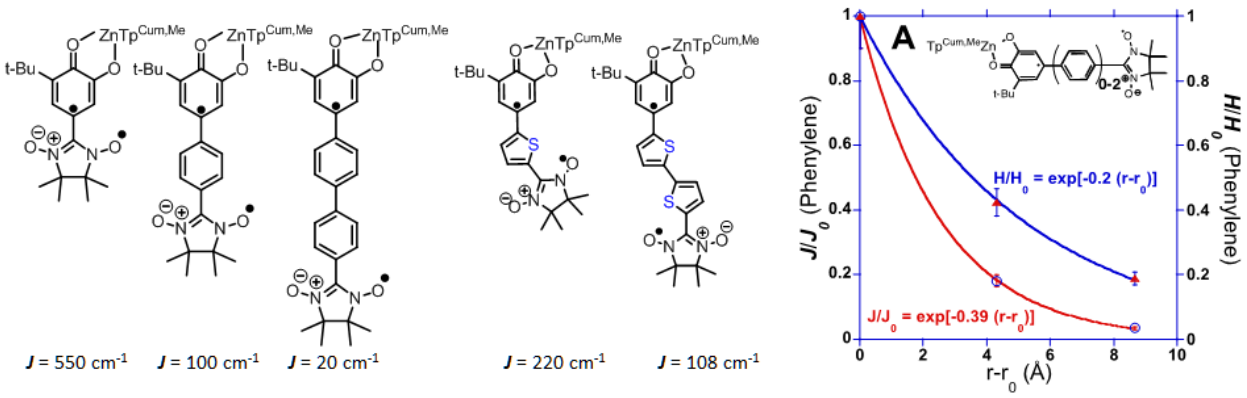


**Figure III.1.** SQ-Bridge-NN molecules used in distance dependence study with bridges oligo(*para*-phenylene), $\beta = 0.39$ Å$^{-1}$ and oligo(2,5-thiophene), $\beta = 0.22$ Å$^{-1}$. A) Correlation between $J$ measured by variable-temperature magnetic susceptibility and bridge distance determined by X-ray crystallography.

**III.2. Torsional Dependence Studies.**

Other past work done by the Shultz group involves synthesizing $Tp^{Cum,Me}Zn$(SQ-B-NN) molecules while varying the $\pi$-system torsion of the bridging unit. Using phenyl bridges with increasing amount of substitution as shown in Figure III.2, The Shultz group created a series of molecules with their $\pi$-system sterically rotated out-of-plane by differing degrees.[2] Measuring their respective *J*-values, the Shultz group found both the $\sigma$- and $\pi$-orbital contributions to the exchange and electronic couplings. Contributions from the $\pi$-system typically dominate electronic contributions between donor and acceptor, but torsional distortions of the $\pi$- system effectively inhibit $\pi$-resonance delocalization and dramatically reduce the magnitude of the electronic coupling between donor and acceptor. Their experimental measurements found that when the bridging $\pi$-system is orthogonal to the donor and acceptor the $\pi$-contribution to electronic and magnetic couplings is zero, and a weak $\sigma$-only pathway dominates. They saw excellent correlation to calculated values. Interestingly, the work is able to measure the donor-bridge and bridge-acceptor contributions to torsion and provides a basis for calculations of torsional dependence to be performed on future molecules.

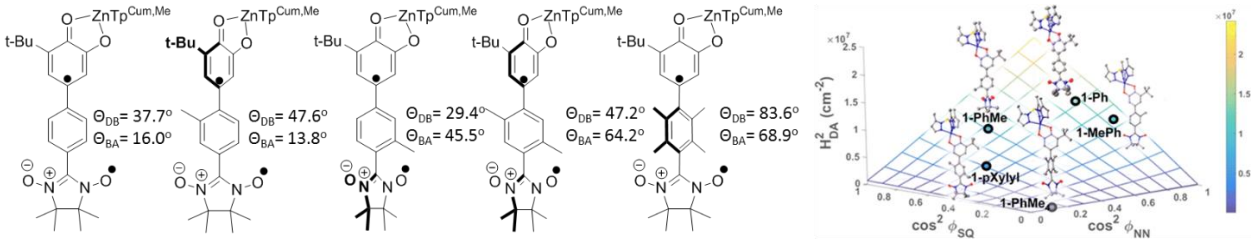


**Figure III.2.** Bond line drawing of SQ-Bridge-NN molecules synthesized in Shultz torsion study. Donor-bridge and bridge-acceptor bond angles measured by x-ray crystallography are given and plotted vs. respective experimentally determined $H_{DA}$ values in a "Ramachandran-type" plot.

## REFERENCES

(1) Kirk, M. L.; Shultz, D. A.; Stasiw, D. E.; Lewis, G. F.; Wang, G.; Brannen, C. L.; Sommer, R. D.; Boyle, P. D. *J. Am. Chem. Soc.*, **2013**, 135, 17144.

(2) Stasiw, D. E.; Zhang, J.; Wang, G.; Dangi, R.; Stein, B. W.; Shultz, D. A.; Kirk, M. L.; Wojtas, L.; Sommer, R. D. *J. Am. Chem. Soc.* **2015**, 137, 9222–9225.

# Chapter IV

## Impact of Vinyl- and Ethynyl- bridges on Electronic Coupling

## IV.1 Vinyl- and Ethynyl- bridges in Shultz Architecture

Carbon-carbon double bonds, as well as their triple bond counterparts, are often used as structural components of bridges in organic based devices. They are attractive to serve as electron transfer bridges due to conjugation with the π-bond, synthetic availability, and moderate- to strong electronic coupling. There are, however, distinct differences between these two fundamental functional groups. Ethynyl bridges have shorter bond lengths and allow free rotation of the π-system, while vinyl groups have slightly longer bond lengths, are less electronegative, and introduce differing steric effects. Interestingly, while double bonds and triple bonds are often used for the same electronic purposes, there is little direct comparison of their electronic coupling. The Shultz biradical approach can provide a direct comparison between these two functional groups complete with their structural and conformational effects. It is likely that the vinyl group will have a stronger coupling value due to better orbital overlap and mixing as explained in Figure IV.1 due to the vinyl group being less electronegative. As Kushmerick suggests, the triple bond breaks the π-system alternation more than a double bond which further indicates that the vinyl group has stronger coupling.[1] Work done by Kiguchi involving

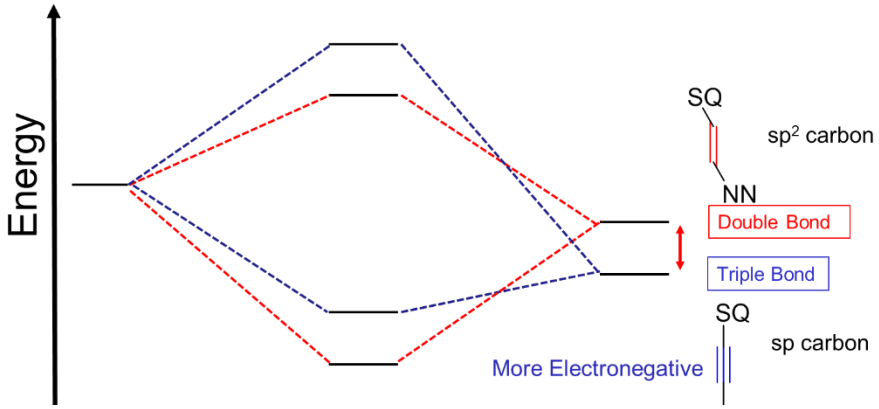


**Figure IV.1.** Generic orbital energy diagram mixing a generic orbital of higher energy with both double and triple bonds. Triple bonds are more electronegative, and therefore lower lying than double bonds, but better mixing can provide additional stabilization for double bond systems.

conductance studies of ethylene and acetylene in the gas phase suggests that vinyl groups do

have a stronger coupling compared to ethynyl groups.[2] Chang, *et al.*, found in a comparison of non-linear optic properties between trans-stilbene and diphenylacetylene, that the vinyl bridge molecule showed larger second-order polarizability ($\beta$) and third-order hyperpolarizability ($\gamma$) than the acetylene for every donor-acceptor pair they studied.[3] Polarizability in simple terms is a degree of charge separation in the ground state further providing a link between ground-state structure and electronic effects. Changes in bond length alternation (BLA) should also be an indicator of stronger or weaker coupling when comparing vinyl or ethynyl bridges as BLA stems from the energy gap between donor and acceptor. Stronger coupling, or a weaker energy gap, decrease the magnitude of bond length alternation and such an effect should also be seen in the series of molecules proposed in Figure IV.2.

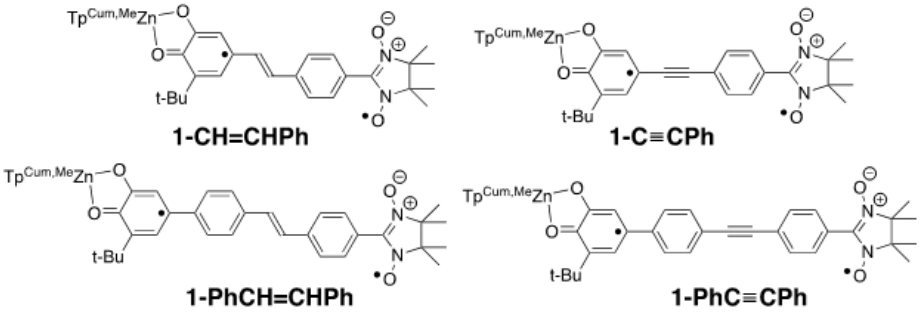


**Figure IV.2.** Compounds proposed for ethene- and ethyne-bridged biradicals.

Synthetic routes are based on those of previous group members' work and attempted synthetic procedures can be found in further detail in Section IV.3. Phenyl rings were chosen to act as spacers between vinyl and acetyl groups and the NN acceptor in order to combat the hydrolysis of the acetylene bridge which oxidizes to a ketone seen in Figure IV.3. This oxidation occurs during the bishydroxylamine cyclization step in the classical Ullman synthetic procedure.[5] Dehydrobromination of the brominated vinyl bridge, however, is a successful route to the

directly bonded acetylene-NN moiety and will be useful for future experimentation. Comparison between the mono-phenyl bridged biradicals should provide interesting magnetic (*J*) and

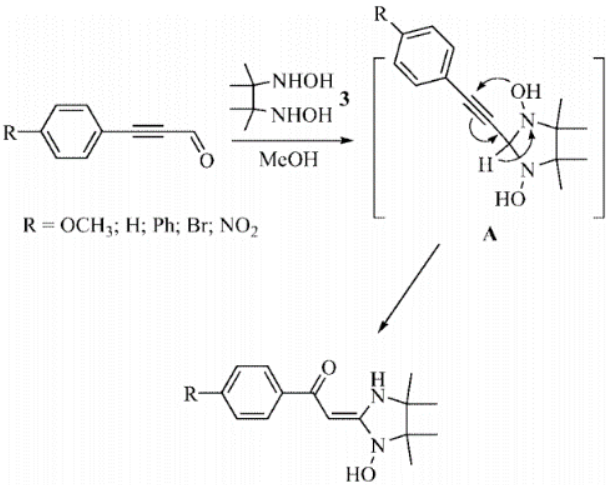


**Figure IV.3.** Mechanism of acetylene hydrolysis during bishydroxlamine cyclization step.

electronic ($H_{DA}$) coupling values and yield the first direct comparison of coupling between a vinyl and ethynyl single-molecule bridge, albeit as styryl and phenylethynyl groups. Further, comparing mono-phenyl to their diphenyl counterparts should elucidate interesting BLA properties and serve as another source of verification of the previous distance dependence work done by the Shultz group.

Synthesis of the $ZnTp^{cum,me}$ ancillary ligand proved challenging due to unanticipated problems and it appeared that the general Shultz biradical architecture was not needed to quantify the electronic delocalization of double and triple bonds. Therefore, a monoradical approach was taken. The monoradical compounds forgo the $ZnTp^{cum,me}$ and NN radical in favor of a simpler complexation with KH to yield the SQ potassium salt. Unfortunately, crystallization of the potassium salt proved difficult and therefore, we are unable to obtain X-ray structures of these molecules. They are still worth studying due to their ability to emulate the Shultz architecture and they can provide useful results.

## IV.2 Monoradical Vinyl- and Ethynyl Bridges

Analyzing the electron delocalization, particularly of the SQ radical into a bridge, is not limited to using only the Shultz biradical archetype. The stretching frequencies ($\mathcal{V}$) of both vinyl $\mathcal{V}_{(CH=CH)}$ and acetyl $\mathcal{V}_{(C\equiv C)}$ functional groups are modulated by the amount of electron delocalization of the SQ radical in the molecules proposed in Figure IV.4A. Since the bond

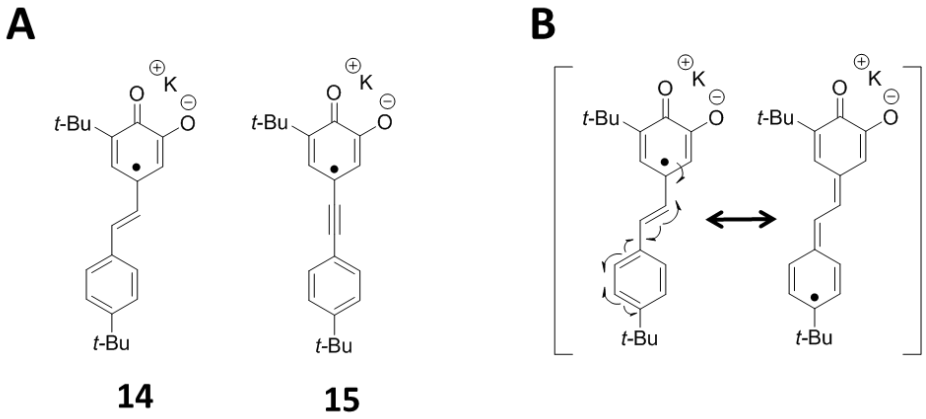


**Figure IV.4.** A) Proposed molecules for studying vinyl $\mathcal{V}_{(CH=CH)}$ and acetyl $\mathcal{V}_{(C\equiv C)}$ stretching frequencies. B) Resonance structures of radical delocalizing through π system.

length of the vinyl or acetylene group is changed through delocalization of the radical, a function easily explained by inspecting resonance structures as seen in Figure IV.4B, the amount of change is proportional to the amount of delocalization. This means that the functional group which displays the greatest ratio of change of $\mathcal{V}$, has the greater electron delocalization, and will indicate which functional group has a stronger coupling value. The region of the estimated vinyl and ethynyl stretching frequencies is 1620-1680 $cm^{-1}$ and 2100-2260 $cm^{-1}$ respectively. Unfortunately, all attempts at discerning them using infrared spectroscopy (IR) were unsuccessful. The vinyl $\mathcal{V}_{(CH=CH)}$ most likely is overlapping with other stretches within that region. Raman spectroscopy was more successful although it only Compound **1** has been fully studied. Raman spectrum of the *trans*-double bond quinone, catechol, and semi-quinone are shown below. Interestingly, there is no apparent $\mathcal{V}_{(CH=CH)}$ stretch. This indicates a significant

amount of electron delocalization into the double bond which causes the stretching frequency to shift and be coincident with other vibrations. This data suggests a large coupling value for the double bond bridge although its precise value is still unclear. This does show, however, that double bonds are quite useful for applications seeking strong coupling values such as electron transfer systems. The UV-Vis and Raman spectrum of **12, 13,** and **14,** is shown in Figure IV.5. Resonance Raman was performed on **14** as 442nm incident light is within resonance range. Synthetic discussion of these molecules and their triple bond counterparts can be found in Section IV.3.

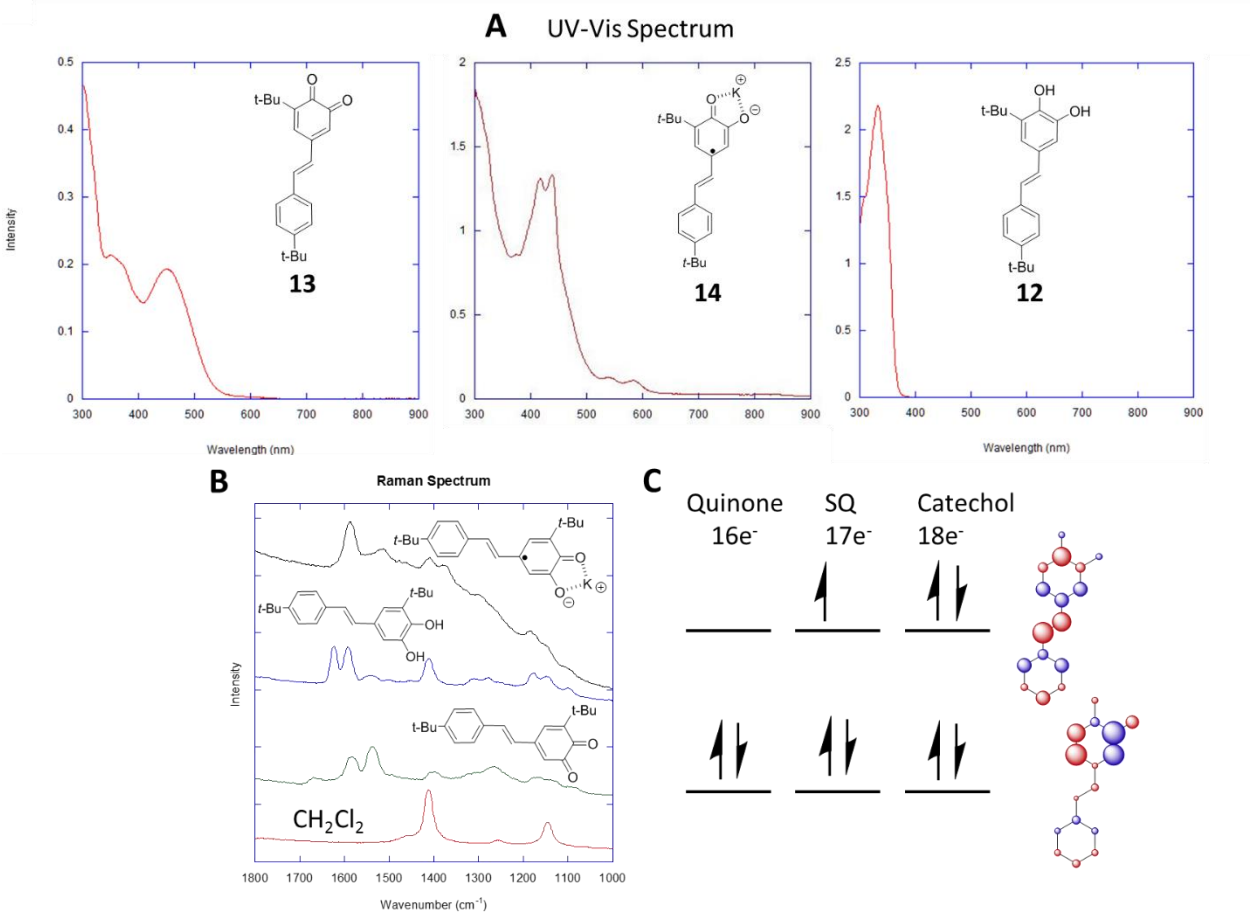


**Figure IV.5.** A) UV-Vis spectrum performed in DCM. B) Raman Spectrum of KSQ, Catechol, Quinone, and DCM solvent. 442nm λ. C) Simple-Huckel molecular orbital calculations of $\pi$-system HOMO.

**IV.3 Synthesis of Monoradicals**

A series of compounds lacking the $Tp^{Cum,Me}Zn^{+}$ complex ion and instead oxidizing a catechol to the SQ using KH were proposed in an effort to assess SQ delocalization. Synthesis of $K^{+}SQ^{-}$ simply requires mixing of equimolar amounts of quinone and catechol together in the presence of a small excess of KH. The potassium ion to complexes with the catechol/quinone mixture which if in a perfect equilibrium, equilibrates to a S = ½ SQ. Potassium salts of SQs are air-sensitive and have short lifetimes requiring characterization to be carried out anaerobically and in a timely manner. A *tert*-butyl-terminated phenyl group was chosen to limit possible reactions at the para position which contains non-zero spin/charge density. The ethynyl bridge synthesis originally proposed was based on Gary Farmer's previous work using Sonogashira coupling methods combining phenylacetylene and $MOM_2$CatBromide (**1**) Figure IV.6A.

Unfortunately, repeating Gary's work was unsuccessful most likely due to the difficulty of removing impurities from the bromide starting material even while in a colorless crystalline form. Additionally, carbon-carbon bond-forming reactions are known to be very sensitive to specific substrate-leaving group combinations and having bromide on the electron rich MOM-protected catechol yielded no reaction contrary to Gary's previous work. Table IV.1 lists the attempted Sonogashira coupling conditions. Synthesis of the TMS-protected acetylene was also attempted in conjunction with $MOM_2$CatBromide (**1**) to test if the phenyl ring was the cause of poor reactivity but with all $MOM_2$CatBromide (**1**) experiments run, only starting material was recovered.

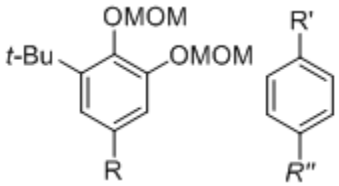


R' = -C≡CH, I

R = -C≡CH, Br  R'' = -CHO, *t*Bu, H

**Table IV.1.** Various Sonogashira coupling reactions performed with CuI, and deoxygenated/degassed solvents under $N_2$.

| R | R’ | R” | Catalyst | Base | Solvent | Temp | Time | Micro wave | Result |
|---|---|---|---|---|---|---|---|---|---|
| Br | C≡CH | CHO | $Pd(PPh_3)_4$ | Piperidine | Piperidine | 80℃ | 12h | no | No RXN |
| Br | C≡CH | CHO | $Pd(PPh_3)_4$ | Piperidine | Piperidine | 80℃ | 24h | no | No RXN |
| Br | C≡CH | *t*Bu | $Pd(PPh_3)_4$ | Piperidine | Piperidine | 80℃ | 24h | no | No RXN |
| Br | C≡CH | H | $Pd(PPh_3)_4$ | Piperidine | Piperidine | 80℃ | 24h | no | No RXN |
| Br | C≡CH | *t*Bu | $Pd(PPh_3)_4$ | $Et_3N$ | THF | 120 ℃ | 1h | 200W | No RXN |
| Br | C≡CH | *t*Bu | $Pd(PPh_3)_4$ | $Et_3N$ | THF | 120 ℃ | 3h | 200W | No RXN |
| Br | C≡CH | *t*Bu | $Pd(PPh_3)_2Cl_2$ | $Et_3N$ | THF | 120 ℃ | 1h | 200W | No RXN |
| Br | C≡CH | *t*Bu | $Pd(PPh_3)_4$ | $Et_3N$ | Toluene | 120 ℃ | 1h | 200W | No RXN |
| C≡CH | I | *t*Bu | $Pd(PPh_3)_4$ | $Et_3N$ | THF | 25℃ | 12h | no | 94%, |

A more successful route than starting with using the $MOM_2CatBromide$ (**1**) and performing Sonogashira coupling, was found by using $MOM_2CatAldehyde$ (**3**) produced by performing a lithium halogen exchange of the bromide. This product can be easily purified by

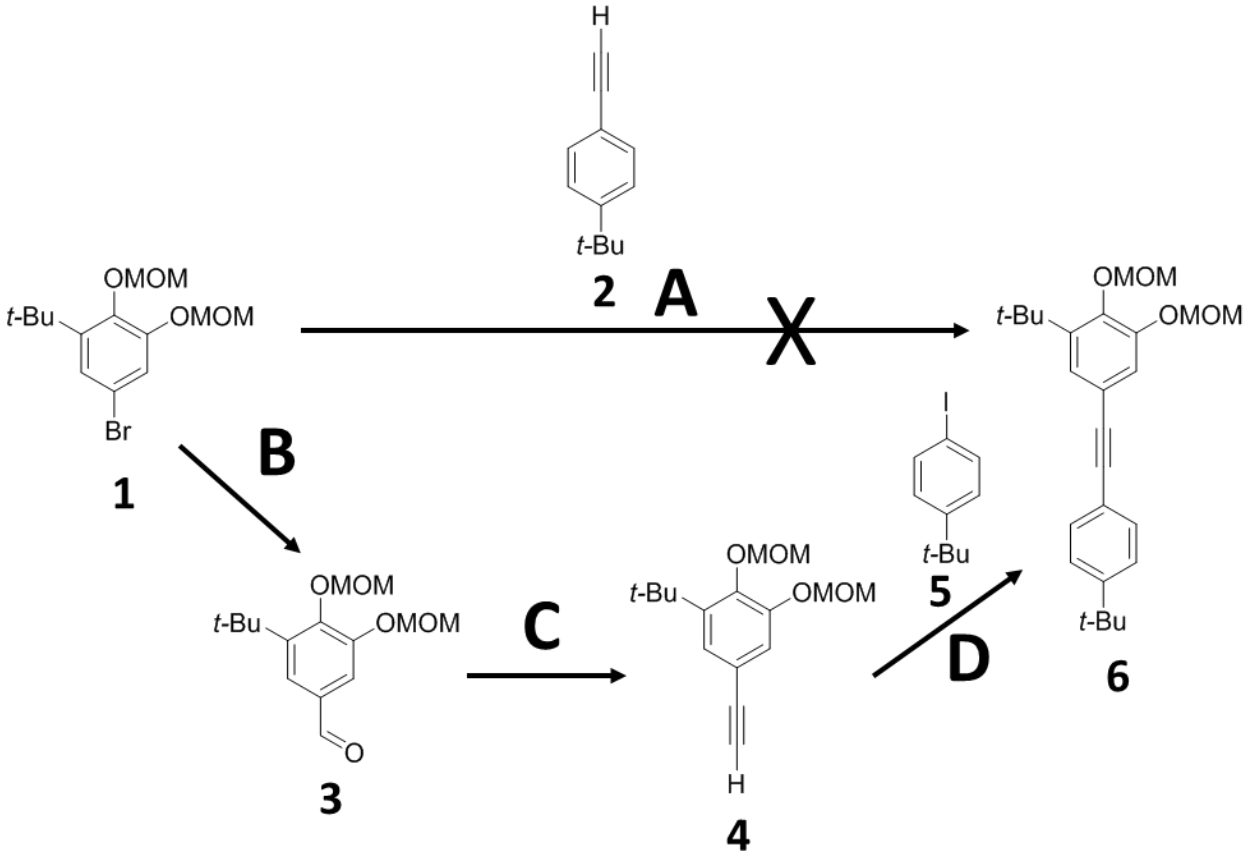


**Figure IV.6.** Synthetic procedure of **6**. A) Sonogashira conditions, B) Lithium halogen exchange, C) Oriha-Bestmann reaction, D) Sonogashira conditions.

column chromatography. The aldehyde was then converted to an acetylene using an Ohira-Bestmann approach and subsequently coupled with 4-iodo-*tert*-butylbenzene (**5**) via Sonogashira conditions at room temperature to yield the MOM-protected bridge. Deprotection of the MOM protecting groups proved difficult as the general procedure of stirring the substrate in acidic conditions caused hydrolysis of the triple bond to form a ketone (**7**). A ketone C=O stretch is evident in the IR spectrum at 1709 $cm^{-1}$ and was a key indicator of triple bond hydrolysis. Because of this hydrolysis, milder deprotection conditions were required to form the catechol

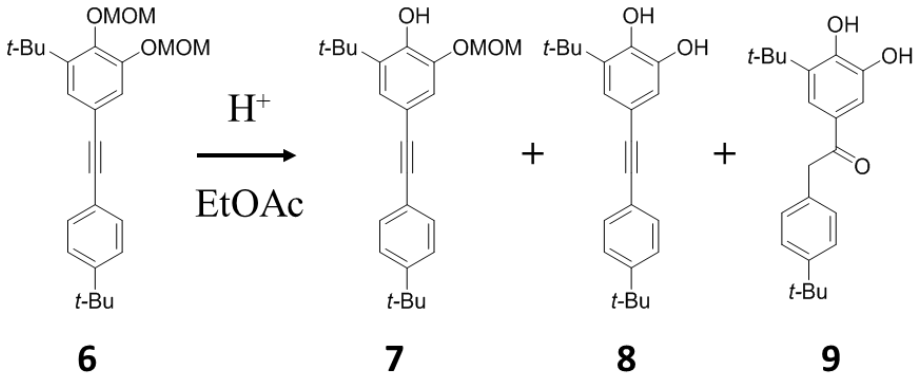


**Figure IV.7.** Deprotection of 4-*tert*-butylphenylacetylene-$MOM_2$catehol (**6**).

which can then be used to continue to complex to the Zn ion in the future steps. Fortunately, all deprotection products are able to be separated by chromatography and can be seen on silica gel TLC with 25% EtOAc/Hexanes as eluent. TLC stains also helped in elucidation of the best conditions as the expected catechol product stains orange in $FeCl_3$ while the hydrolyzed product stains dark purple in $FeCl_3$. Additionally, the hydrolyzed product is bright orange indicating a ketone when staining with DNP. The attempted deprotection conditions are summarized in Table IV.2.

**Table IV.2.** Attempted MOM-deprotection steps on the acetylene bridge. All performed in Anhydrous MeOH under $N_2$.

| Molecule | Deprotection agent | Temp | Time | Result |
|---|---|---|---|---|
| 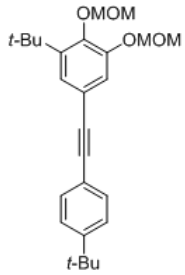 | Anhydrous HCl 1.25M in MeOH | 25℃ | 1h | **6, 7** |
| | Anhydrous HCl 1.25M in MeOH | 25℃ | 3h | **6, 7, 8, 9** |
| | PPTS (pyridium p-toluenesulfonte) | Reflux | 1h | **7, 9** |
| | PPTS | 25℃ | 1h | **7, 9** |
| | PTSA | Reflux | 1h | **6, 7, 8** |
| | PTSA | Reflux | 3h | **6, 7, 8, 9** |
| | PTSA | Reflux | 5h | **6, 7, 8, 9** |
| | PTSA | 25℃ | 1h | **6, 7, 8** |
| | PTSA | 25℃ | 3h | **6, 7, 8** |
| | PTSA | 25℃ | 5h | **7, 8** |

Optimal conditions for deprotection were found to be *p*TSA in MeOH for 5 hours at RT. This yielded a mix of both mono-MOM protected, and fully deprotected product which was expected to be able to easily separate on a column. Unfortunately, all attempts at chromatographic separation/purification produced only the hydrolyzed compound (both mono-protected and catechol). We believed that the column conditions used were too acidic causing hydrolysis and more basic conditions such as treating the silica gel with $Et_3N$ should be attempted in the future. At the time of writing, due to the difficulty in isolating the ethynyl bridge, the vinyl bridge was deemed of more interest and its synthetic procedure was finished.

Vinyl bridge synthesis was initiated from a Wittig reaction using $MOM_2$CatAldehyde (**3**) and 4-*tert*-butylbenzyltriphenylphosphonium bromide (**10**) to yield both *trans*- and *cis*-MOM-protected isomers (**11**) in a ~ 60:40 *trans:cis* ratio. The *cis* isomer readily isomerizes in ambient

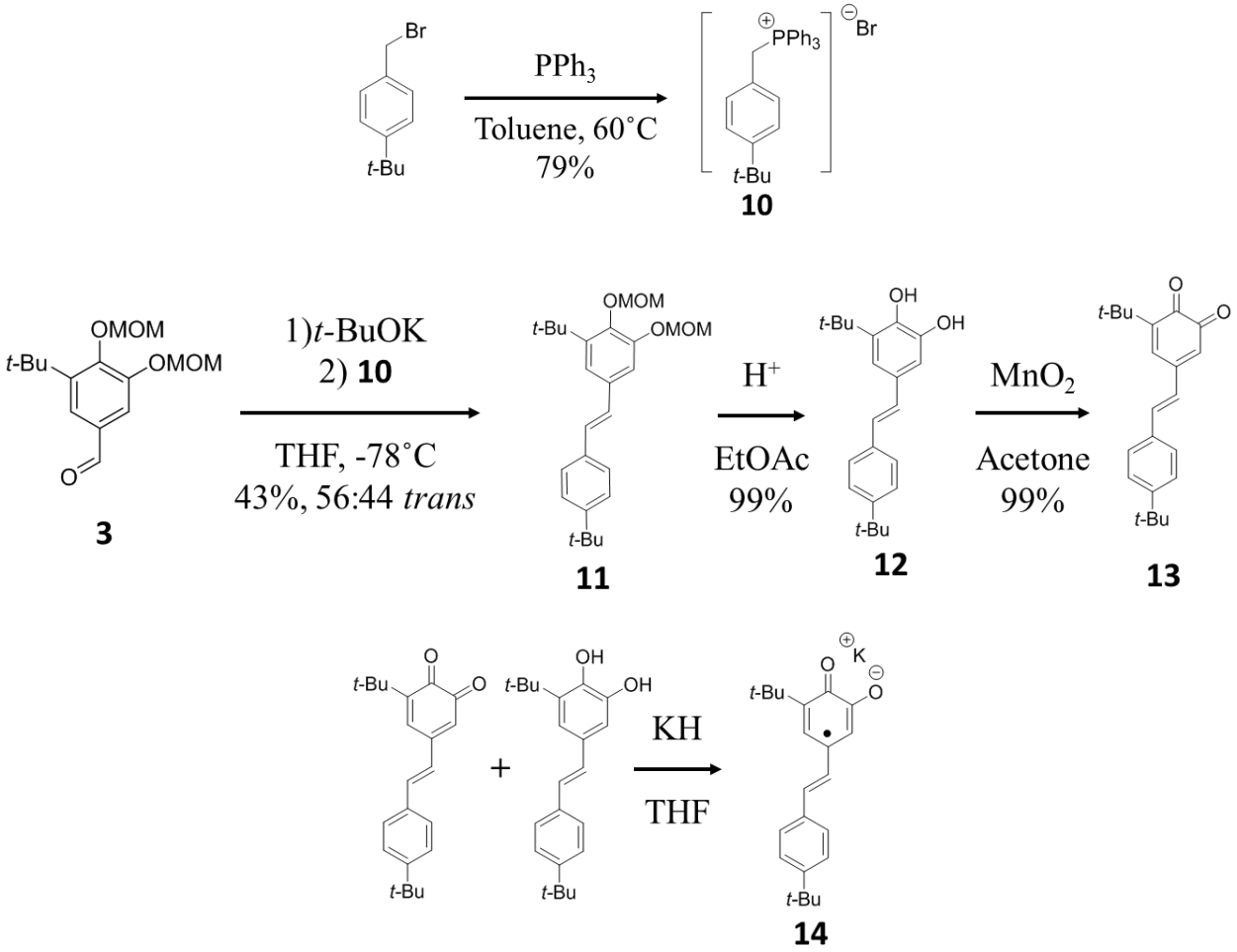


**Figure IV.8.** Synthetic procedure of KSQ vinyl bridge (**14**).

light while the *trans* isomer does not. Isomerization studies can be found in Appendix A. Both isomers can be isolated by chromatography in both MOM-protected and unprotected forms creating two separate synthetic steps to be able to separate them. As such, they can be independently studied. The cis isomers' phenyl ring is understood to be rotated slightly, decreasing potential delocalization through the molecule and isolating the electron density on the SQ. Using samples of both *cis* and *trans* vinyl monoradicals, we can directly probe their

coupling constants through spectroscopy. This is an area study for future efforts as only the *trans* isomer has yet to be fully characterized. Attempts at correlating a simulated single radical species to the experimental data were very effective using WINSIM. Relevant proton coupling constants are given in Table IV.3. Comparing the CH=CH coupling constants with the *cis* isomer is an area of future study as well.

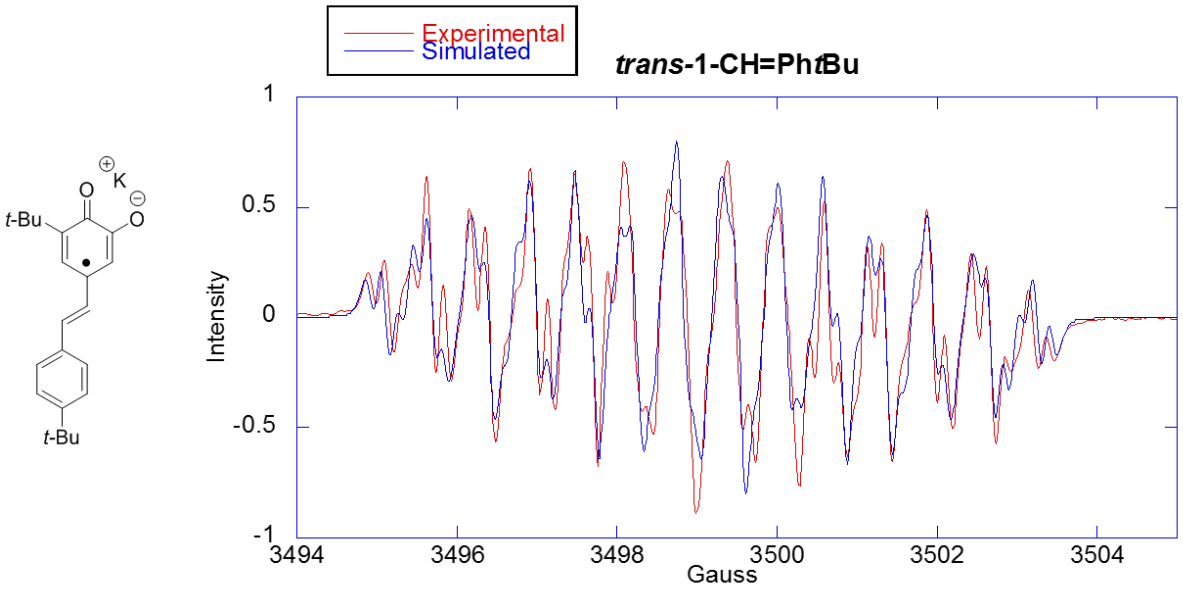


**Figure IV.9.** Experimental and simulated EPR spectrum of **14**.

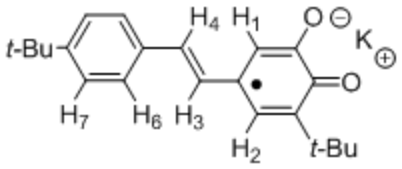


**Table IV.3.** Proton Coupling Constants for compound **14.**

| Proton | Hyperfine Coupling Constant (G) |
|---|---|
| $H_1$ | 1.31 |
| $H_2$ | 3.08 |
| $H_3$ | 0.51 |
| $H_4$ | 1.67 |
| $H_6$ | 0.75 |
| $H_7$ | 0.17 |

## IV.4 Conclusion and Future Work

Steady progress has been made towards understanding the nature of electronic coupling through fundamental functional groups, double and triple bonds. Using SQ radicals in an attempt to measure electron delocalization through the moieties of interest, this work lays the foundation for the study of the underlying electron delocalization properties of vinyl and ethynyl bridges. Vinyl bridged molecules showed significant coupling values indicated by a large shift of the $\nu_{(CH=CH)}$ stretch. The preliminary results of this investigation have interesting implications for molecular design that incorporates vinyl and ethynyl bridges.

Direct comparison of vinyl and ethynyl bridges using the Shultz biradical system are still needed to determine the explicit *J* and $H_{DA}$ coupling values of these fundamental moieties. Using debromination of the dibromovinyl bridge, an acetylene covalently bonded to a NN radical can be synthesized. This overcomes the limitation of forming a ketone due to the oxidation of the terminal oxygen. This, in conjunction with the phenylethyl-bridged donor-acceptor-biradicals, will illuminate the true nature of their respective electronic coupling.

Comparing *cis* and *trans* isomers of the vinyl bridge moiety should provide another interesting data point in determining the effect of a vinyl bridge coupling. Due to the slight rotation of the *cis* isomer causing the phenyl ring to be rotated out of plane, the coupling should be different through the double bond as more electron density is localized on the SQ ring. Analyzing this will help applications that still require double bonds as electron bridges but do not have distinctly planar systems.

Additionally, future efforts can be focused on synthesizing directly bonded SQ-bridge-NN biradical systems without a phenyl ring to act as a spacer. This will provide coupling values without any chance of interference from additional variables such as the phenyl ring torsions.

Also, comparison of $^{1}H$ NMR between cis and trans vinyl catechols and their respective catecholate versions allow provide us with coupling constants for the vinyl protons and therefore their electron density differences as it changes based on the isomer.

## IV.5 Experimental

**General Considerations.** Reagents and solvents were purchased from commercial sources and used as received unless otherwise noted. $^{1}H$ and $^{13}C$ NMR spectra were recorded on a Varian Mercury 400 MHz or a Varian Mercury 300 MHz spectrometer at room temperature. $^{1}H$ and $^{13}C$ chemical shifts are listed in parts per million (ppm) and are referenced to residual protons or carbons of the deuterated solvents, respectively. EPR spectra were recorded on an IBM ER200D-SRC EPR spectrometer in $CH_2Cl_2$. Infrared spectra were recorded on a Brüker Vertex 80V spectrometer with Brüker Platinum ATR attachment. Elemental analyses were performed by Atlantic Microlabs, Inc. Mass spectra were obtained at the NCSU Mass Spectrometry Facility located in the Department of Chemistry.

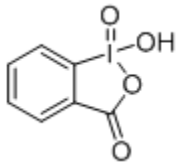


**2-iodoxybenzoic acid (IBX).** 2-iodobenzoic acid (81.08 g, 327 mmol) was added to a 2000 mL over dried round bottom flask. Potassium peroxymonosulfate (OXONE, 416.25 g, 667 mmol) was then added to the flask and dissolved with 300 mL $H_2O$. The mixture was mechanically stirred and heated to 80 $^{\circ}C$ for three hours. The mixture was then removed from heat and cooled to 0 $^{\circ}C$ with continued stirring in a NaCl/ice bath for one hour. The resulting precipitate was filtered through a Büchner funnel and washed with 1000 mL deionized $H_2O$ and 200 mL acetone. A colorless solid was collected and left to dry open to air overnight to yield **1** (80.85 g, 91%). Characterization data was consistent with that reported in the literature. ref. 6.

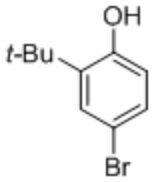


**4-bromo-2-(*tert*-butyl)phenol.** 2-(*tert*-butyl)phenol (29.0 g, 0.270 mmol) was charged to an oven-dried 250 mL round-bottom flask with stir bar and dissolved in 120 mL of dichloromethane. The flask was fit with an addition funnel and a drying-tube then chilled to -40 °C. Liquid bromine (40.96 g, 0.29 mol) was poured into the dripping funnel, diluted with $CH_2Cl_2$ and added to the chilled reaction solution dropwise. Upon completion the reaction was stirred and allowed to warm to room temperature overnight. The reaction was then quenched with water and transferred to a separatory funnel, diluted with diethyl ether, and washed with brine and sodium bicarbonate. The solution was then dried over sodium sulfate then concentrated to yield **1** (55.2 g, 90%) as a dark red oil. Characterization data was consistent with that reported in the literature. ref. 7


**Chloromethyl methyl ether.** Hexanoyl chloride (270.85 g, 2.01 mol) was added to a 500 mL nitrogen-purged oven dried round bottom flask with a stir bar. A dripping funnel was attached to the flask and the solution cooled to 0 °C in a NaCl/ice bath. Once cool, dimethoxymethane (165 mL, 1.86 mol) was added dropwise over one hour. Following dropwise addition, the reaction was allowed to stir for an additional 3 hours at 0 °C. Reaction was followed by $^1H$ NMR in $CDCl_3$. Upon full conversion of dimethoxymethane, the solution is distilled at 60 °C. After discarding initial runoff, **2** is collected as a colorless liquid (132.72 g, 89%). Characterization data was consistent with that reported in the literature. ref. 8.

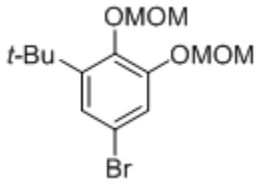


**5-bromo-1-(tert-butyl)-2,3-bis(methoxymethoxy)benzene (1).** 4-bromo-2-(*tert*-butyl)phenol (13.27 g, 58 mmol) was charged to an oven-dried 250 mL round-bottom flask with stir bar, and dissolved in 60 mL dichloromethane and 20 mL methanol. 2-Iodoxybenzoic acid (24.29, 87 mmol) was added to the mixture and allowed to stir for 30 min. The solvent was removed and the oil was dissolved in hexanes, passed through a silica pad (1.5 cm height / 6 cm diameter), and eluted with hexanes. The filtrate was concentrated under reduced pressure and a red-brown solid was isolated. The isolated red-brown solid was dissolved in a mixture of 50 ml acetone and 50 ml $H_2O$. The solution was cooled to 0 $^{\circ}$C and sodium dithionite (8.61 g, 49 mmol) was added. The mixture was stirred at 0 $^{\circ}$C until pale yellow then transferred to a separatory funnel, diluted with diethyl ether, washed with brine and the organic layer was then dried over sodium sulfate. The solution was concentrated under reduced pressure to give a yellow oil. The oil was dissolved in hexanes, passed through a silica pad and eluted with hexanes. The eluent was then concentrated under reduced pressure yielding catechol (4.95g, 19 mmol) as a yellow oil. The oil was transferred to a nitrogen-purged oven-dried 100 mL 2-neck round-bottom flask with stir bar, dissolved in 40 mL of dichloromethane and chilled to 0 $^{\circ}$C. Chloromethyl methyl ether (3 mL g, 39 mmol) was added to the reaction solution at 0 $^{\circ}$C then *N*,*N*-diisopropylethylamine (7 mL, 40 mmol) was added to the mixture dropwise. Following the dropwise addition the solution was stirred at 0 $^{\circ}$C for 30 min before being refluxed overnight. The reaction mixture was diluted and transferred to a separator funnel with diethyl

ether, washed with ammonium chloride then brine, dried over $Na_2SO_4$, then passed through a silica pad and eluted with diethyl ether and dried over sodium sulfate. The solution was concentrated under reduced pressure as a dark red oil. The solution was then further concentrated bulb to bulb via a Kügelrohr apparatus and yielded a yellow oil which was then crystallized in hexanes at 0 °C resulting in **1** (2.36 g, 7 mmol, 12%) as a colorless solid. Characterization data was consistent with that reported in the literature. ref. 7.

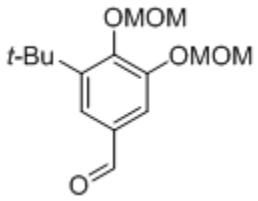


**3,4-Bis(methoxymethoxy)-5-tert-butylbenzaldehyde (3).** (0.9933 g, 2.98 mmol) was added to a 50 mL oven dried round bottom flask. The flask was sealed with a rubber stopper and purged/pumped with $N_2$ three times. 30 mL of dried THF was added and the flask was cooled under $N_2$ to -78 °C in a dry ice/acetone bath. Once cool, *tert*-butyllithium (3.8 mL, 6.46 mmol) was added dropwise through syringe. Once fully added, the reaction solution was stirred 15 minutes. Anhydrous and deoxygenated DMF (0.7 mL, 9 mmol) was added dropwise through a syringe and the reaction was stirred 30 additional minutes at -78 °C. The solution was then allowed to warm to room temperature over 2 hours. Deoxygenated $H_2O$ was added the reaction and the solution was stirred overnight. The solution was concentrated under reduced pressure and passed through a silica gel column deprotected with $Et_3N$ and eluting with 10% ethyl acetate/hexanes to yield **5** (.8324 g, 99%) as a colorless oil. Characterization data was consistent with that reported in the literature. ref. 9.

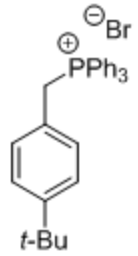


**4-*tert*-Butylbenzyltriphenylphosphonium bromide (10).** Triphenylphosphine (2.31 g, 8.8 mmol) was charged to a 100 mL round-bottom flask with a stir bar. 20 mL toluene was added to dissolve. 1-Bromomethyl-4-*tert*-butylbenzene (1.981 g, 8.7 mmol) was added. A reflux condenser was attached, and the flask was heated to 60 ˚C and stirred for 4 hours. The resulting precipitate was filtered through a Büchner funnel and washed with $Et_2O$. Yielded **10** (3.7398g, 88%) as a white solid. Characterization data was consistent with that reported in the literature. ref. 10.

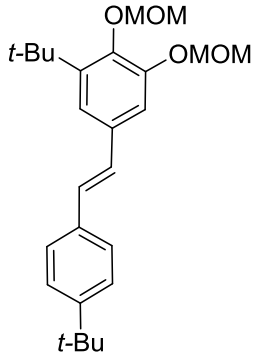


**(*E*)-1-(*tert*-butyl)-5-(4-(*tert*-butyl)styryl)-2,3-bis(methoxymethoxy)benzene (11).** 4-*tert*-Butylbenzyltriphenylphosphonium bromide (2.086 g, 4.2 mmol) was added to a 50 mL oven dried round bottom flask with stir bar and purged with $N_2$. Anhydrous potassium *tert*-butoxide (1.00 g, 8.9 mmol) was added to the flask. The flask was sealed under $N_2$ and cooled to -78 ºC in a dry ice/acetone bath. 20 mL dried THF was added to dissolve. Compound **5** (1.059 g, 3.7 mmol) was added dropwise through syringe. A reflux condenser was attached, and the solution

was heated to 60 ˚C for 24 hours. The resulting reaction was then transferred to a separatory funnel and washed with NaCl. The organic layer was extracted and dried over $Na_2SO_4$ then loaded onto a silica gel column and eluted with hexanes. Yields **11** (0.7527 g, 43%) in a 56:44 *trans*:*cis* ratio. The *trans* compound is a colorless solid while the *cis* compound is a colorless oil. $^1$H NMR (400 MHz, chloroform-d) δ (ppm): 7.4315 (d, *J* = 8.59 Hz, 2H), 7.3605 (d, *J* = 8.59 Hz, 2H), 7.205 (d, *J* = 1.96 Hz, 1H), 7.121 (d, *J* = 2.34 Hz, 1H), 7.002 (d, *J* = 16.4 Hz, 1H), 6.9495 (d, *J* = 16.4 Hz, 1H), 5.2145 (d, *J* = 8.43 Hz, 4H), 3.653 (s, 3H), 3.536 (s, 3H), 1.444 (s, 9H), 1.324 (s, 9H).

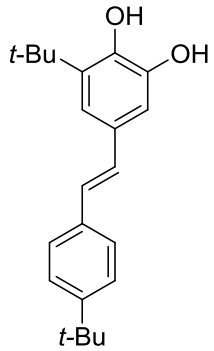


**(*E*)-3-(*tert*-butyl)-5-(4-(*tert*-butyl)styryl)benzene-1,2-diol (12). 7** (0.0526 g, 0.127 mmol) was charged to a 25 mL round bottom flask with stir bar. 5 mL of ethyl acetate was added to dissolve and 1-2 drops of 12 M HCl was added dropwise. The reaction was stirred overnight in ambient conditions. The resulting product was then transferred to a separatory funnel and washed with NaCl three times. The organic layer was extracted and dried over $Na_2SO_4$ then loaded onto a silica gel column and eluted first with 100% hexanes and then ramped up to 20%EtOAc/hexanes to yield **14** (0.0409 g, 99%) as a colorless solid. $^1$H NMR (400 MHz, chloroform-d) δ (ppm): 7.401 (d, *J* = 8 Hz, 2H), 7.3475 (d, *J* = 8.4 Hz 2H), 6.928 (m, 4H). $^{13}$C ($CDCl_3$) δ (ppm): 29.5, 31.3, 34.6, 110.1, 118.8, 125.52, 125.91, 126.18, 127.98, 128.9, 134.8,

136.5, 142.9, 150.3. IR v($cm^{-1}$): 3631, 3464, 3405, 3310, 2961, 2901, 2869, 1592, 1513, 1428, 1360, 1310, 1176, 967, 848.

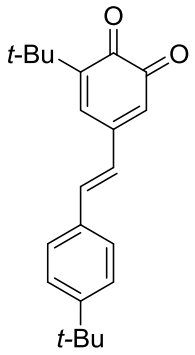


**(*E*)-3-(*tert*-butyl)-5-(4-(*tert*-butyl)styryl)cyclohexa-3,5-diene-1,2-dione (13)**. **14** (0.0067 g, 0.0206 mmol) was charged to a 4 mL vial with stir bar. 1mL of acetone was added to dissolve and a spatula tip of $MnO_2$ was added. Reaction was followed by silica plate TLC in 10%EtOAc/hexanes. After completion of reaction (30 min - 1 hr) product was passed through a pad of celite and eluted with acetone. The solution was concentrated under reduced pressure to yield **13** (0.0066 g, 99%) as a dark red solid. $^1$H NMR (400 MHz, chloroform-d) δ (ppm):

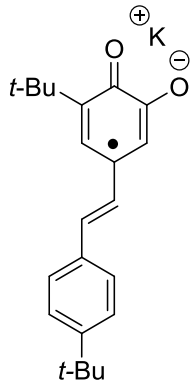


KSQ (**14**): **12** (0.0092 g, 0.0283 mmol) and **13** (0.0051 g, 0.0276 mmol) were added to a 4 mL vial with stir bar. The flask was purge pumped with $N_2$ and placed into a glovebox where KH (0.101 g, 0.755 mmol) 30% by weight in mineral oil was added. 1 mL of THF was added to

dissolve and the reaction was stirred for 5 minutes. Dark red solution containing the SQ was sealed in $N_2$ and further characterized.

## REFERENCES

(1) J. Kushmerick; *et. Al. J. Am. Chem. Soc.*, **2002**, 124 (36), 10654–10655.

(2) Kiguchi, M; *et al. J. Phys. Chem. C*., **2012**, 116, 18250−1825.

(3) Chang L. T., *et al., J. Phys. Chem*. **1991,** 95, 10643.

(4) Chang L. T., *et al., J. Phys. Chem*. **1991,** 96, 10631.

(5) Tretyakov, E. *Eur. J. Org. Chem*. **2006**, 2695–2702

(6) Magdziak, D.; Rodriguez, A. A.; Van De Water, R. W.; Pettus, T. R. R. *Org. Lett*. **2002**, 4, 285.

(7) Shultz, D. A.; Hollomon, M. *G. Chem. Matter*. **2000,** 12, 580-585

(8) Berliner, Martin A.; Belecki, Katherine. *J. Org. Chem.*, **2005**, 70 (23), 9618–9621.

(9) Shultz, D.A.; Bodnar, S.H.; Vostrikova, K.E.; Kampf, J.W. *Inorg. Chem.* **2000**, 39, 6091-6093.

(10) Cui, M, *et al. European Journal of Medicinal Chemistry.* **2011**, 46, 2908-2916.

# APPENDIX

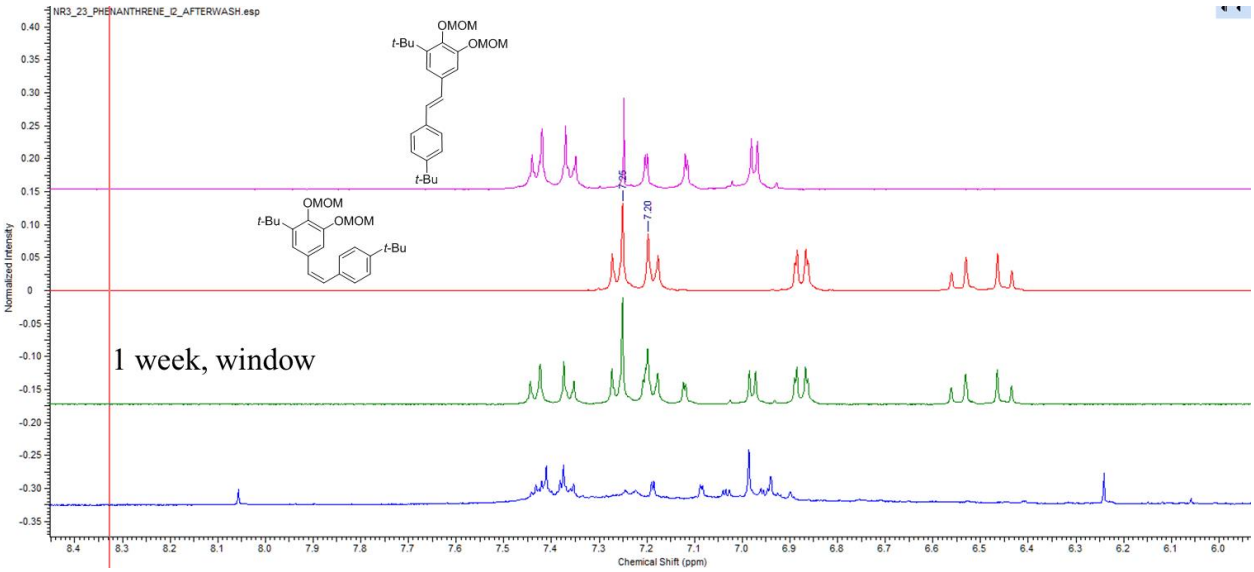


**Figure A.i.** NMR spectrum of pure *cis*-**14** after (green) one week in sunlight, and (blue) oxidation with $I_2$ stirred in EtOAc for 24 hours. *Cis*-**14** (red) and *trans*-**14** (pink) provided as reference.